POLITECNICO
MILANO 1863

SCUOLA DI INGEGNERIA INDUSTRIALE
E DELL'INFORMAZIONE

Executive Summary of the Thesis

High-order discontinuous Galerkin methods for 1D vascular flows: from single-scale models to 3D-1D multiscale haemodynamics

Laurea Magistrale in Aeronautical Engineering - Ingegneria Aeronautica

Author: Pietro Businaro

Advisor: Prof. Luca Dede'

Co-advisor: Dr. Michele Bucelli

Academic year: 2024-2025

1. Introduction

One-dimensional (1D) modeling of the vascular flow [1] is extensively employed in literature to study the pressure waveforms within arteries, since it is notably less expensive with respect to the three-dimensional (3D) counterpart. In this work, we present the underlying mathematical formulation of the 1D haemodynamics equations and devise a suitable numerical technique, adopting discontinuous Galerkin (DG) methods for the space discretization and explicit Adams-Bashforth (AB) time-stepping schemes. For numerical modeling purposes, the literature assumes a flat velocity profile when writing the momentum transport term, since this leads to considerable mathematical simplifications. In this work, we avoid this hypothesis by deriving Roe's linearization [2] for the 1D blood flow equations, in order to compute the intercell fluxes appearing in the DG framework. The entire implementation is written in C++ and carried out within the `life`[x]* project.

*https://lifex.gitlab.io/lifex-public/

2. Mathematical modeling

The 1D haemodynamics equations read [1]:

$$\begin{cases} \dfrac{\partial A}{\partial t} + \dfrac{\partial Q}{\partial x} = 0 \\ \dfrac{\partial Q}{\partial t} + \dfrac{\partial (\alpha Q^2/A)}{\partial x} + \dfrac{A}{\rho}\dfrac{\partial P}{\partial x} + K_R \dfrac{Q}{A} = 0 \end{cases} \quad (1)$$
$$\forall x \in \Omega = (x_L, x_R),\ \forall t \in (0, t_f]\ ,$$

where x_L and x_R represent the left and right endpoint of the 1D domain, while t_f is the final time. The unknowns are represented by A (i.e. the cross-sectional lumen area) and Q (i.e. the volumetric flow rate). ρ is the blood density, while α represents the momentum flux correction factor: $\alpha := \frac{\int_S \rho u_x^2 \mathrm{d}S}{\rho u^2 A}$. The axial velocity u_x is approximated by assuming a suitable velocity profile, namely $u_x(x, r, t) \approx u(x, t)\ s\left(\frac{r}{R(x,t)}\right)$, where the normalized velocity profile is given by: $s\left(\frac{r}{R}\right) = \frac{\gamma+2}{\gamma}\left[1 - \left(\frac{r}{R}\right)^{\gamma}\right]$. Common choices for γ include $\gamma = \{2, 9\}$ [3]. K_R is a coefficient modeling the wall shear stress: $K_R = -2\pi\nu\ \frac{\mathrm{d}s}{\mathrm{d}r}\big|_{r=R}$, with $\nu = \frac{\mu}{\rho}$ being the kinematic viscosity. The tube law is given by:

$$P(x,t) = P_{\text{ref}} + \beta\ \frac{\sqrt{A} - \sqrt{A_{\text{ref}}}}{A_{\text{ref}}}\ , \quad (2)$$

where P_{ref} and A_{ref} are the reference pressure and area, while $\beta := \frac{\sqrt{\pi}hE}{1-\xi^2}$ represents the wall properties (h is the wall thickness, E the Young modulus and ξ the Poisson ratio). We denote the wave speed by $c := \sqrt{\frac{A}{\rho}\frac{\partial P}{\partial A}} = \sqrt{\frac{\beta}{2\rho A_{\text{ref}}}} A^{\frac{1}{4}}$.

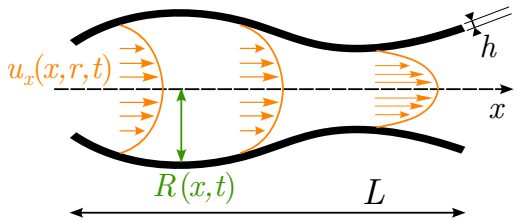

Figure 1: Straight blood vessel.

The mathematical model (1) can be further rearranged in order to obtain the *quasi-linear form*:

$$\begin{aligned} &\frac{\partial \mathbf{U}}{\partial t} + \mathrm{H}(\mathbf{U})\frac{\partial \mathbf{U}}{\partial x} + \mathbf{B}(\mathbf{U}) = \mathbf{0} \\ &\forall x \in \Omega = (x_L, x_R),\ \forall t \in (0, t_f]\ , \end{aligned} \tag{3}$$

and the *conservative form*:

$$\begin{aligned} &\frac{\partial \mathbf{U}}{\partial t} + \frac{\partial \mathbf{F}(\mathbf{U})}{\partial x} + \mathbf{S}(\mathbf{U}) = \mathbf{0} \\ &\forall x \in \Omega = (x_L, x_R),\ \forall t \in (0, t_f]\ , \end{aligned} \tag{4}$$

with $\mathbf{U} = (A, Q)^\top$ being the unknowns, $\mathrm{H}(\mathbf{U})$ the Jacobian matrix, $\mathbf{F}(\mathbf{U})$ the fluxes, and $\mathbf{B}(\mathbf{U})$, $\mathbf{S}(\mathbf{U})$ the reaction terms, collecting the viscous contribution. Under physiological conditions, this hyperbolic problem is in a subcritical state, meaning that it is characterized by two waves traveling in opposite directions.

3. Numerical modeling

3.1. Space and time discretizations

The space discretization is achieved by means of DG methods. The weak formulation applied to the conservative form (4) reads [4]:

$$\begin{aligned} \sum_{m=1}^{M} \Bigg\{ \left(\frac{\partial \mathbf{U}_h}{\partial t}, \mathbf{v}_h\right)_{\Omega_m} - \left(\mathbf{F}(\mathbf{U}_h), \frac{\mathrm{d}\mathbf{v}_h}{\mathrm{d}x}\right)_{\Omega_m} + \\ + \left(\mathbf{S}(\mathbf{U}_h), \mathbf{v}_h\right)_{\Omega_m} \Bigg\} + \\ + \sum_{e=1}^{E} \mathbf{F}^*(\mathbf{U}^e_{h,L}, \mathbf{U}^e_{h,R}) \cdot (\mathbf{v}^e_{h,L} - \mathbf{v}^e_{h,R}) = 0 \\ \forall \mathbf{v}_h \in V_h\ , \end{aligned} \tag{5}$$

where $\mathbf{F}^*(\mathbf{U}^e_{h,L}, \mathbf{U}^e_{h,R})$ is the *numerical flux*, describing the flux term at the interface between two consecutive cells. The time discretization is achieved by applying explicit AB schemes [4]. Given the hyperbolic nature of the problem at hand, a Courant-Friedrichs-Levy (CFL) restriction on the time step is necessary to ensure the stability of the numerical method. The initial data are projected onto V_h by means of L^2-projection.

3.2. Numerical flux and Riemann problem

At the interface between two consecutive cells, a Riemann problem is defined, meaning that we must solve a wave propagation problem with piecewise constant initial conditions:

$$\mathbf{U}(x, t^n) = \begin{cases} \mathbf{U}^e_L & \text{if } x < x^e \\ \mathbf{U}^e_R & \text{if } x > x^e \end{cases} \tag{6}$$

and constant boundary conditions, equal to $\mathbf{U}^e_L$ and $\mathbf{U}^e_R$, while the unknowns are given by the intermediate state $\mathbf{U}^{*e}$ and the corresponding numerical flux $\mathbf{F}^*(\mathbf{U}^e_L, \mathbf{U}^e_R)$, as depicted in Figure 2.

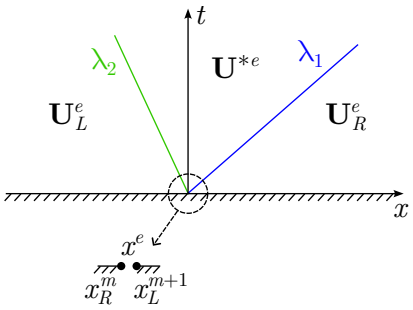

Figure 2: Graphical representation of the Riemann problem.

The literature assumes $\alpha = 1$ for numerical modeling purposes, since, in that case, we have at our disposal an analytical expression for the characteristic variables and so the definition of the numerical flux $\mathbf{F}^*(\mathbf{U}^e_L, \mathbf{U}^e_R)$ is straightforward [4]. The novelty of this work lies in devising a numerical technique that avoids this hypothesis, allowing $\alpha \neq 1$ to be chosen consistently with the selected velocity profile (i.e. $\alpha = \frac{\gamma+2}{\gamma+1}$). This is achieved by applying Roe's linearization [2] to the 1D haemodynamics equations, yielding:

$$\frac{\partial \mathbf{U}}{\partial t} + \widetilde{\mathrm{H}}\,\frac{\partial \mathbf{U}}{\partial x} = \mathbf{0}\ , \tag{7}$$

where $\widetilde{\mathrm{H}} = \widetilde{\mathrm{H}}(\mathbf{U}^e_L, \mathbf{U}^e_R) = \mathrm{H}(\widetilde{A}, \widetilde{Q}, \widetilde{c})$ is the linearized (constant-coefficient) Jacobian matrix,

while $\widetilde{A}, \widetilde{Q}, \widetilde{c}$ are called *Roe's averages*, chosen to guarantee the local conservation of the problem, formally: $\widetilde{\mathrm{H}}\left(\mathbf{U}_R^e - \mathbf{U}_L^e\right) = \mathbf{F}(\mathbf{U}_R^e) - \mathbf{F}(\mathbf{U}_L^e)$. The expression for Roe's averages is derived specifically in this work and results in:

$$\begin{aligned} \widetilde{A} &= \left(\frac{\sqrt{A_L^e} + \sqrt{A_R^e}}{2}\right)^2 , \\ \widetilde{Q} &= \frac{\sqrt{\widetilde{A}}}{2}\left(\frac{Q_L^e}{\sqrt{A_L^e}} + \frac{Q_R^e}{\sqrt{A_R^e}}\right) , \\ \widetilde{c} &= \sqrt{\frac{\beta}{2\rho A_{\text{ref}}}\frac{A_L^e + \sqrt{A_L^e A_R^e} + A_R^e}{3\sqrt{\widetilde{A}}}} . \end{aligned} \tag{8}$$

By solving the Riemann problem for the linearized system (7), we obtain the following approximation for the intermediate state $\mathbf{U}^{*e}$:

$$\mathbf{U}^{*e} = \mathbf{U}_L^e + \left[\widetilde{\mathbf{l}}_2 \cdot \left(\mathbf{U}_R^e - \mathbf{U}_L^e\right)\right] \widetilde{\mathbf{r}}_2 , \tag{9}$$

and for the numerical flux $\mathbf{F}^*(\mathbf{U}_L^e, \mathbf{U}_R^e)$:

$$\mathbf{F}^*(\mathbf{U}_L^e, \mathbf{U}_R^e) = \mathbf{F}(\mathbf{U}_L^e) + \widetilde{\lambda}_2 \left[\widetilde{\mathbf{l}}_2 \cdot \left(\mathbf{U}_R^e - \mathbf{U}_L^e\right)\right] \widetilde{\mathbf{r}}_2, \tag{10}$$

where $\widetilde{\lambda}_2$, $\widetilde{\mathbf{l}}_2$, $\widetilde{\mathbf{r}}_2$ represent the second eigenvalue, the second left eigenvector and the second right eigenvector of $\widetilde{\mathrm{H}}$, respectively.

3.3. Boundary conditions and inverse Riemann problem

The Riemann problem also arises at the boundary, where we can identity an internal state $\mathbf{U}^{-e}$, known by interpolation of the latest solution, and an external state $\mathbf{U}^{+e}$, representing a virtual state outside the domain. A visualization is offered in Figure 3 for the left endpoint of the domain x_L, where we highlight that $\mathbf{U}^{+e}$ and $\mathbf{U}^{-e}$ are indeed linked to $\mathbf{U}_L^e$ and $\mathbf{U}_R^e$.
At the boundary nodes, the unknowns are given by both the intermediate state $\mathbf{U}^{*e}$ and the external state $\mathbf{U}^{+e}$, leading to the following *inverse Riemann problem* in 4 equations and 4 unknowns:

$$\begin{cases} g(A^{*e}, Q^{*e}) = 0 \\ \mathbf{U}^{*e} = \mathbf{U}_L^e + \widetilde{\mathbf{r}}_2 \left[\widetilde{\mathbf{l}}_2 \cdot \left(\mathbf{U}_R^e - \mathbf{U}_L^e\right)\right] \\ A_L^e = A_R^e \end{cases} \tag{11}$$

The residual $g(A^{*e}, Q^{*e}) = 0$ is defined based on the specific boundary condition, meaning that

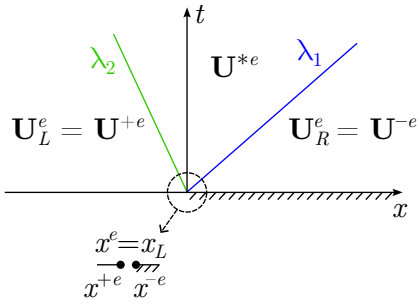

Figure 3: Graphical representation of the inverse Riemann problem.

the non-linear system (11) can be employed to introduce an arbitrary boundary condition in a flexible way. The choice to enforce the continuity of the cross-sectional area between the internal and external state (i.e. $A^{-e} = A^{+e}$ or, equivalently, $A_L^e = A_R^e$) is arbitrary, since the external state $\mathbf{U}^{+e}$, is virtual and has no physical meaning.
The implemented boundary conditions include:

- *inlet:* we prescribe a known value of a certain quantity over time, which can be either the cross-sectional area (i.e. $A^{*e} = A_{\text{in}}(t)$), the inflow (i.e. $Q^{*e} = Q_{\text{in}}(t)$) or the pressure (i.e. $P^{*e} = P_{\text{in}}(t)$);
- *non-reflecting:* we require the outgoing waves to leave the computational domain without any wave reflection, formally:

$$\mathbf{l}_{\text{in}}(\mathbf{U}^{*e}) \cdot \left[\frac{\partial \mathbf{U}^{*e}}{\partial t} + \mathbf{S}(\mathbf{U}^{*e})\right] = 0 , \tag{12}$$

  with $\mathbf{l}_{\text{in}}$ being the left eigenvector of $\mathrm{H}(\mathbf{U})$ associated with the incoming characteristic; (12) is discretized in time by means of a forward Euler scheme;
- *3-element Windkessel model:* this lumped-parameter model is employed to represent the peripheral circulation and consists in a proximal resistance R_1, a compliance C and a distal resistance R_2; the constitutive law is expressed by:

$$\begin{aligned} &R_2 C \frac{\mathrm{d}P^{*e}}{\mathrm{d}t} + P^{*e} - P_{\text{out}} = \\ &= R_1 R_2 C \frac{\mathrm{d}Q^{*e}}{\mathrm{d}t} + (R_1 + R_2)\, Q^{*e} , \end{aligned} \tag{13}$$

  where P_{out} is the outflow pressure; we discretize (13) by means of a backward Euler scheme.

4. Extension to blood vessel networks

The model discussed so far is suitable to simulate one single isolated vessel. A network of vessels may include points where the material properties are discontinuous. If we consider two consecutive compartments "1" and "2" (i.e. portions of the vessel with different material properties), then we can enforce the continuity of the flow rate and the total pressure at the interface between these two compartments, formally:

$$Q_1^{*e} = Q_2^{*e} \,, \qquad P_{\text{tot},1}^{*e} = P_{\text{tot},2}^{*e} \,, \tag{14}$$

with $P_{\text{tot}} := P + \frac{1}{2}\rho u^2 = P + \frac{1}{2}\rho \left(\frac{Q}{A}\right)^2$. The corresponding inverse Riemann problem is illustrated in Figure 4.

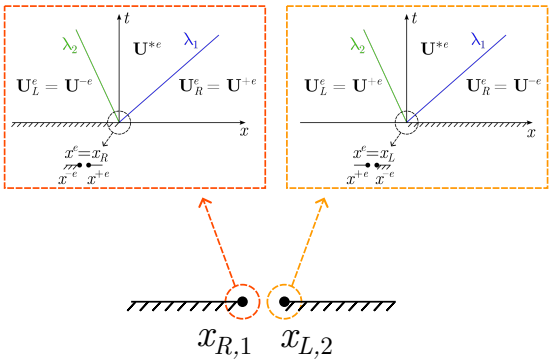

Figure 4: Graphical representation of the inverse Riemann problem at discontinuous material points.

By following a similar approach, we can also model the bifurcation points (Figure 5), i.e. points where one single vessel divides into two separate vessels, yielding the matching conditions:

$$Q_1^{*e} = Q_2^{*e} + Q_3^{*e} \,, \quad P_{\text{tot},1}^{*e} = P_{\text{tot},2}^{*e} = P_{\text{tot},3}^{*e} \,. \tag{15}$$

5. 3D-1D coupling

5.1. Some notes about the 3D FSI formulation

The 3D FSI problem is simulated using the `life`$^{\text{x}}$ built-in solver. The fluid subproblem is expressed in an arbitrary Lagrangian-Eulerian (ALE) framework, in order to deal with moving boundaries. We employ the Saint Venant-Kirchhoff constitutive model for the structure

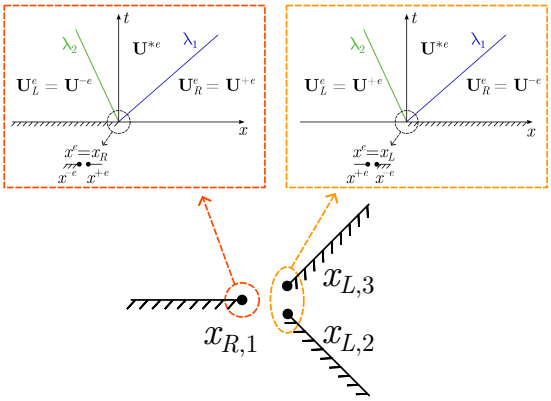

Figure 5: Graphical representation of the inverse Riemann problem at bifurcation points.

subproblem. A continuous Galerkin finite element formulation is adopted for both the fluid and the structure subproblems, with 1$^{\text{st}}$-order Lagrange polynomials as basis functions. The time discretization is obtained by means of 2$^{\text{nd}}$-order implicit backward differentiation formula (BDF) schemes. SUPG-PSPG stabilization is used to avoid artificial checkerboard patterns in the pressure. Concerning the boundary conditions, in this work we consider a known pressure at the fluid inlet and a non-reflecting boundary condition at the fluid outlet, expressed as follows:

$$\mathrm{T}_f \,\mathbf{n}\Big|_{t^{n+1}} = -R_t \, Q_{3\mathrm{D}} \,\mathbf{n}\Big|_{t^n} \qquad \forall \mathbf{x} \in \Gamma_{f,\text{out}} \tag{16}$$

with $\mathrm{T}_f = -P_{3\mathrm{D}}\mathbb{I} + \mu\left(\nabla \mathbf{u}_{3\mathrm{D}} + (\nabla \mathbf{u}_{3\mathrm{D}})^\top\right)$ being the stress tensor for the fluid subproblem. R_t represents the terminal resistance: $R_t = \frac{\rho c_0}{A_0}$, with c_0 and A_0 being the initial wave speed and cross-sectional area, respectively. Concerning the structure subproblem, we allow the structure to move radially by means of homogeneous Neumann boundary conditions, while the normal displacement is set to zero.

5.2. Coupling conditions

The coupling between the 3D FSI model and the 1D blood flow model is achieved by means of suitable coupling conditions. We employ an explicit coupling strategy, meaning that no subiteration is performed within the same time step. In this case, the numerical stability at the coupling interface is ensured if we enforce the con-

tinuity of the pressure on the 3D FSI problem:

$$\begin{aligned}(\mathrm{T}_f\,\mathbf{n})\cdot\boldsymbol{\tau}_1 &= 0\\ (\mathrm{T}_f\,\mathbf{n})\cdot\boldsymbol{\tau}_2 &= 0\\ (\mathrm{T}_f\,\mathbf{n})\cdot\mathbf{n} &= -P_{1\mathrm{D}}\Big|_{\Gamma_{3\mathrm{D}\text{-}1\mathrm{D}}}\end{aligned} \tag{17}$$

Again, for the structure subproblem, we keep homogeneous Neumann boundary conditions radially, while the normal displacement is enforced to be null. Concerning the 1D haemodynamics model, the coupling condition reads:

$$W_{\mathrm{in}}(A^{*e},Q^{*e})\Big|_{\Gamma_{3\mathrm{D}\text{-}1\mathrm{D}},t^{n+1}} = W_{\mathrm{in}}(A_{3\mathrm{D}},Q_{3\mathrm{D}})\Big|_{\Gamma_{f,3\mathrm{D}\text{-}1\mathrm{D}},t^{n}} \tag{18}$$

with W_{in} being the incoming characteristic variable. In the case of Roe's linearization, W_{in} is expressed as: $W_{1,2}\approx\widetilde{\mathbf{l}}_{1,2}\cdot\mathbf{U}$, with $\widetilde{\mathbf{l}}_{1,2}$ being the left eigenvectors of the linearized Jacobian matrix $\widetilde{\mathrm{H}}$. We refer to [5] for a more detailed discussion about the stability of these coupling conditions.

6. Numerical results

6.1. Verification against benchmark solutions

In this section, we replicate the numerical setup considered in [3], in order to verify the current implementation. In particular, we simulate two arteries (*common carotid artery* and *upper thoracic aorta*) and a bifurcation point (*aortic bifurcation*), with a prescribed inflow at the inlet and a 3-element Windkessel boundary condition at the outlet. The geometry and the results are illustrated in Figure 6 and Figure 7, respectively.

6.2. 3D-1D coupling results

In order to evaluate the 3D-1D coupling and the corresponding numerical issues, we study a Gaussian-shaped pressure pulse propagation along a duct, and perform both standalone and coupled simulations. Hence, at the inlet, we enforce the following pressure pulse: $P_{\mathrm{in}}(t)=P_{\max}\exp\left(-a\,(t-t_0)^2\right)$ with a maximum pressure $P_{\max}=2\times10^3\,\mathrm{Pa}$, an attenuation factor $a=10^4\,\mathrm{s}^{-2}$ and a reference time $t=0.05\,\mathrm{s}$. We adopt a non-reflecting boundary condition at the outlet (12)–(16). The coupling conditions are given by (17)–(18). The pressure and flow rate waveforms are plotted in Figure 8, where we highlight the spurious wave reflections

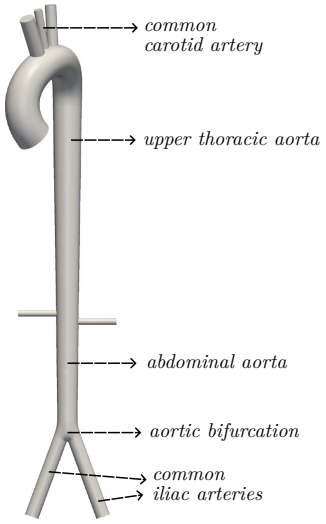

Figure 6: 3D model of an idealized aorta, considering the main branches up to the *aortic bifurcation*, taken from [3].

arising at the coupling interface between the 1D and 3D models at $t=0.10\,\mathrm{s}$ (Figure 8b).

6.3. Convergence analysis

In order to evaluate the convergence rate, we compare the numerical solution with the solution obtained by linearizing (1)–(2) around the reference state $(A,Q,P)=(A_{\mathrm{ref}},0,P_{\mathrm{ref}})$. Indeed, under the hypothesis of small perturbations, the linearized solution can be considered a sufficiently good approximation of the solution of the non-linear system (1). For this purpose, we prescribe a sine wave inflow at the inlet: $Q_{\mathrm{in}}(t)=\widehat{Q}\sin\left(\frac{2\pi}{T}t\right)$ with $\widehat{Q}=10^{-6}\,\mathrm{m}^3/\mathrm{s}$ being the sine wave amplitude and $T=0.1\,\mathrm{s}$ its period. At the outlet, a non-reflecting boundary condition (12) is employed. The errors on the cross-sectional area and on the flow rate are computed in terms of L^2-error norm, and evaluated at the final time $t_f=2.0\,\mathrm{s}$.

It is noteworthy that the h-convergence exhibits a super-convergent regime, where the maximum convergence rate is equal to 4 with polynomials of degree $p=2$, as expected for DG methods on structured grids. The p-convergence shows an exponential decay of the L^2-error norms, as predicted by spectral/hp element methods theory. Concerning the time convergence, only 1^{st}-order convergence is achieved, even though we adopted a 2^{nd}-order AB scheme; in order to obtain the optimal rate of convergence, we should employ a larger time step, but this is not possible due to the numerical instability of AB

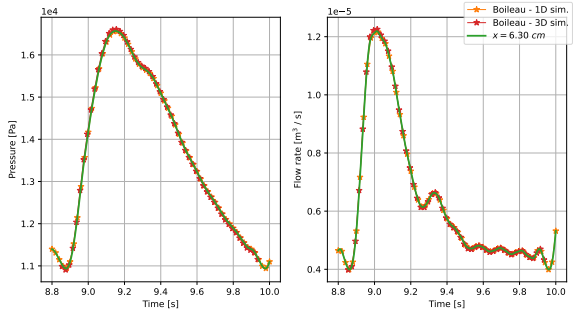

(a) *common carotid artery.*

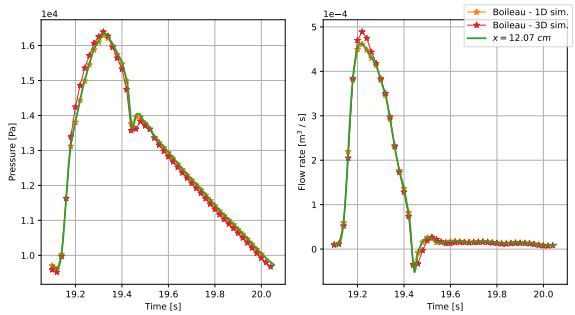

(b) *upper thoracic aorta.*

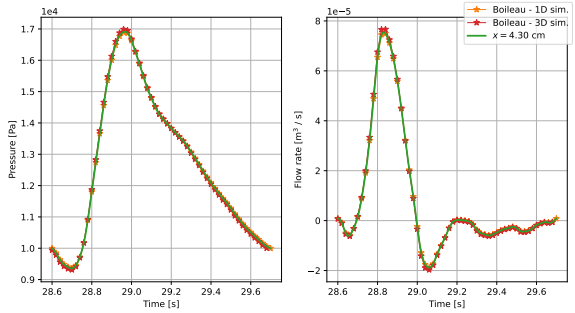

(c) *aortic bifurcation* (*abdominal aorta*).

Figure 7: Pressure and flow rate at the middle point of each blood vessel during the last cardiac cycle. The 1D and 3D simulations taken from [3] are marked with the labels *Boileau - 1D sim.* and *Boileau - 3D sim.*

time steppers (i.e. we can use only time steps satisfying a proper CFL condition).

7. Conclusions and future developments

In this work, we have analyzed the 1D vascular flow model with an arbitrary velocity profile, and its coupling with 3D FSI models. The current implementation has been verified with known results in literature. A preliminary study has been conducted on the 3D-1D coupled simulations, highlighting the spurious wave reflections arising at the coupling interface; this issue

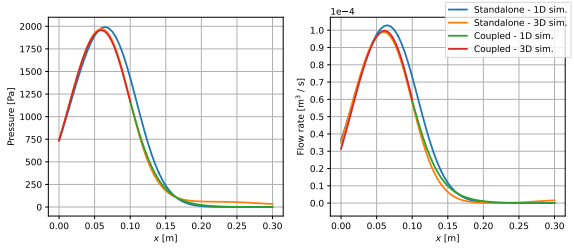

(a) $t = 0.06\,\mathrm{s}$.

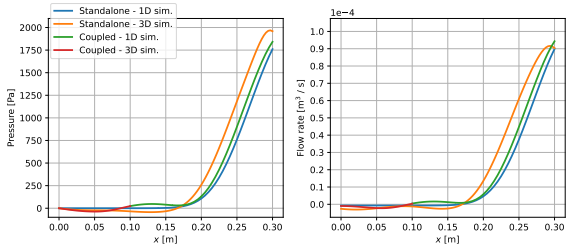

(b) $t = 0.10\,\mathrm{s}$.

Figure 8: Gaussian-shaped waveform along the duct at different time steps. Standalone and coupled simulations are plotted.

should be analyzed more in depth, and can be possibly overcome by implementing additional sub-iterations within the same time step. Finally, the *h*-, *p*- and time convergence has been discussed; it could be interesting to adopt explicit Runge-Kutta (RK) schemes for the time stepping, in order to reach an optimal rate of convergence in time.

References

[1] A. Quarteroni et al. Mathematical Modelling and Numerical Simulation of the Cardiovascular System. In *Computational Models for the Human Body*. 2004.

[2] P.L. Roe. Approximate Riemann solvers, parameter vectors, and difference schemes. *Journal of Computational Physics*, 1981.

[3] E. Boileau et al. A benchmark study of numerical schemes for one-dimensional arterial blood flow modelling. *International Journal for Numerical Methods in Biomedical Engineering*, 2015.

[4] S.J. Sherwin et al. Computational modelling of 1D blood flow with variable mechanical properties and its application to the simulation of wave propagation in the human arterial system. *International Journal for Numerical Methods in Fluids*, 2003.

[5] L. Formaggia et al. On the stability of the coupling of 3D and 1D fluid-structure interaction models for blood flow simulations. *ESAIM: Modélisation mathématique et analyse numérique*, 2007.